LANGMUIR

pubs.acs.org/Langmuir Article

Molecular Insights into the Improved Bioactivity of Interferon Conjugates Attached to a Helical Polyglutamate

Zhuanglin Shen, Yiming Sun, Guoliang Zhu, Gaixia Xu, Zhenqiang Yu, Hua Lu,* and Yantao Chen*

Cite This: *Langmuir* 2023, 39, 6539−6547 Read Online

ACCESS | Metrics & More | Article Recommendations | Supporting Information

ABSTRACT: Attaching polymers, especially polyethylene glycol (PEG), to protein drugs has emerged as a successful strategy to prolong circulation time in the bloodstream. The hypothesis is that the flexible chain wobbles on the protein's surface, thus resisting potential nonspecific adsorption. Such a theoretical framework may be challenged when a helical polyglutamate is used to conjugate with target proteins. In this study, we investigated the structure−activity relationships of polyglutamate-interferon conjugates P(EG_3Glu)-IFN using molecular simulations. Our results show that the local crowding effect induced by oligoethylene glycols (i.e., EG_3) is the primary driving force for helix formation in P(EG_3Glu), and its helicity can be effectively increased by reducing the free volume of the two termini. Furthermore, it was found that the steric hindrance induced by IFN is not conductive to the helicity of P(EG_3Glu) but contributes to its dominant orientation relative to interferon. The orientation of IFN relative to the helical P(EG_3Glu) can help to protect the protein drug from neutralizing antibodies while maintaining its bioactivity. These findings suggest that the helical structure and its orientation are critical factors to consider when updating the theoretical framework for protein−polymer conjugates.

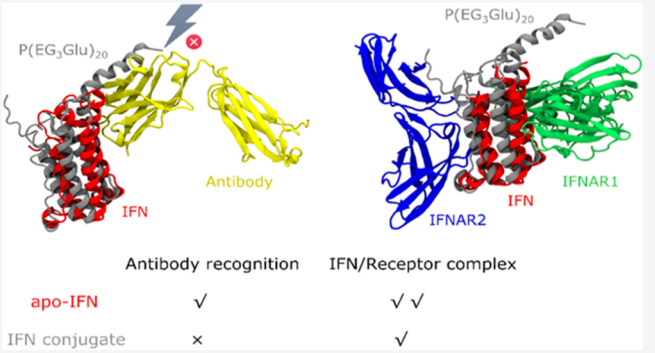

INTRODUCTION

As a modern therapeutic approach, protein drugs exhibit high efficiency and selectivity, while most of them are severely hampered in clinical applications. Multiple obstacles, such as rapid renal clearance, proteolytic degradation, and immune responses, greatly decrease the proteins' circulation time *in vivo*.[1,2] To overcome these limitations, attaching polyethylene glycol (PEG) to the target protein was first proposed by Professor Frank Davis in the late 1970s.[3] Owing to its neutral charge, amphiphilic properties, and hydration capacity, PEG is the most widely used antibiofouling polymer. To date, about 20 protein-PEG conjugates have been approved for marketing as therapeutic drugs.[4]

As known, the flexible PEG can encapsulate the target protein, and wobble on the protein surface, thus shielding it from nonspecific adsorption by proteolytic enzymes, antibodies, and also its receptors.[5] Molecular simulation of PEGylated bovine serum albumin (BSA) revealed the correlation between the molecular weight of the attached PEG and the shelf life of BSA.[6] In addition to PEG, researchers have explored a wide range of attached partners, including zwitterionic polymers,[7,8] glycopolymers,[9] oligo-EGylated poly(meth)acrylates,[10,11] and intrinsically disordered peptides.[12,13] The flexible and unstructured conformation is the common characteristic of all these polymers, which is believed to be entropically unfavored in biofouling events.[14]

However, such an assumption that the coiled polymers perform better lacks solid experimental evidence. It is difficult to experimentally set up a rational control group in which the conjugated polymer analogs show different conformations but share the same chemical composition. For most polymers, it is necessary to change their chemical composition for obtaining different conformation, and vice versa. Recently, the Lu group[14] synthesized a series of poly(amino acid)s with helical or unstructured conformations just by changing the chirality of residues. In particular, the homopolymerization of L-/D-glutamate derivatives containing oligoethylene glycol (i.e., EG_3) as side chains may form helical structures. In contrast, the racemic copolymerization products D,L-P(EG_3Glu) could exist only as coils. They further revealed that the attached helical L-P(EG_3Glu) endows improved binding affinity to the receptor, in vitro antiproliferative activity, and in vivo efficacy to therapeutic proteins, such as interferon (IFN) and human growth hormone.[15] Clearly, the helicity of the attached polymers should be an important control parameter, which is

Received: February 22, 2023
Revised: April 14, 2023
Published: April 26, 2023

https://doi.org/10.1021/acs.langmuir.3c00501
Langmuir 2023, 39, 6539−6547

overlooked in the traditional paradigm of structure−activity relationships.

Obviously, it is difficult for helical polypeptides to surround the target protein or wobble on the protein surface. From the point of view of the structure−activity relationship, many questions need to be explored. For example, does the attached helical polypeptide form a fixed orientation with the target protein IFN? How can the attached helical polypeptide prevent the formation of complexes for IFN with other proteins? Such microscopic questions are suitable to be explored via molecular simulation.[16−21] For example, the attached coiled polymer/polypeptide is revealed to encapsulate the target protein,[17] and sometimes allosterically change the latter's structure.[21] In previous simulation work,[22,23] we showed that, in delivering therapeutic proteins, the hydrophilic zwitterionic peptides with the highest contact preference could be a potential choice. The zwitterionic peptides $(VPKEG)_n$ endow the target protein with better stability and stealth properties by forming a protective shell, thus achieving a balance between protection and subsequent release.[22] As far as we know, no simulations focusing on the structure−activity relationship of protein conjugates attached to a helical polymer/polypeptide have been performed.

Herein, the secondary structures of polyglutamate derivatives and their biological activity after being conjugated to the target protein (interferon) were investigated using molecular simulation, molecular docking, and binding energy analysis. Several systems were simulated in this work: (a) the apo-IFN system denotes the native interferon (IFNα-2A); (b) the conjugate formed by interferon and polyglutamic acid with a chain length of 100, which is noted as Glu_{100}-IFN. The structure of polyglutamate derivatives containing oligoethylene glycol (EG_3) as side chains is illustrated in Figure 1A, which is called L-P$(EG_3Glu)_n$ and further abbreviated as LPG_n-IFN when conjugated with interferon. Details of molecular modeling and molecular dynamics (MD) simulation can be found in the Supporting Information.

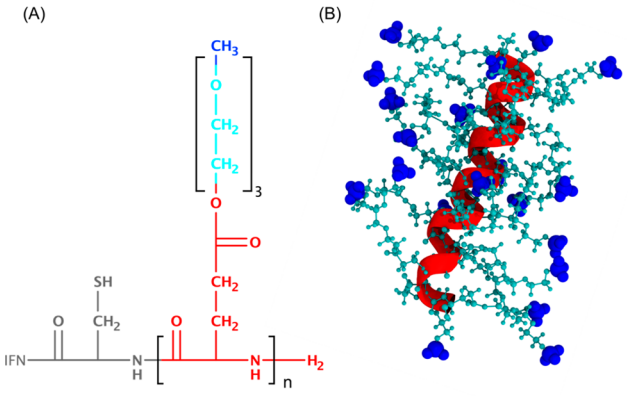

Figure 1. Chemical structure of protein conjugate LPG_n-IFN (A) and typical 3D representation of free polymer LPG_n (n = 20) (B). In (B), the backbone of polyglutamate derivatives is rendered by the red NewCartoon representation. The oligoethylene glycol (EG_3) and terminal methyl group (Me) are rendered by the cyan and blue CPK representation, respectively.

MATERIALS AND METHODS

Construction of the Simulation System. Several simulation systems were constructed, according to the experimental research.[15] The native interferon (IFN-α2A) was first simulated, which is called apo-IFN. The conjugate formed by interferon and polyglutamic acid with a chain length of 100 is called Glu100-IFN. The structure of polyglutamate derivatives containing oligoethylene glycol (EG_3) as side chains is illustrated in Figure 1A, which is called L-P$(EG_3Glu)_n$ and further abbreviated as LPG_n-IFN when conjugated with interferon. Here, n could be 20/50/100/200/400, representing the chain length of polyglutamate derivatives.

The 3D structure of the LPG_n-IFN conjugate molecule is shown in Figure 1B. The initial atomic coordinates of the IFN were selected from the Protein Data Bank (PDB), and the PDB ID is 1ITF. The initial structures of the polypeptides, Glu_{100} and L-P$(EG_3Glu)_n$, were set as α-helices, which formed peptide bonds with the amide group of IFN's first residue Cys^1 of in the conjugate. The associated atomic interactions between residues were described by the classical force field CHARMM36m.[24] Unfortunately, there is no suitable force field to describe the interaction between EG_3 with residues, which was constructed using quantum mechanics (QM) methods (see Parameterization for Polyglutamate Derivatives section). All molecular dynamics simulations were performed via the NAMD software package (ver. 2.14),[25] and other details of simulation systems are listed in Table S1.

Parameterization for Polyglutamate Derivatives. The force field parameters for glutamate derivative EG_3Glu were optimized using the ffTK plugin of VMD software.[26] The atom types for the glutamic and EG_3 side chains are derived from CHARMM36m and CGenFF,[27] respectively. The molecular structures of glutamate derivative EG_3Glu was optimized at the MP2/6-31G* level of theory by ORCA,[28] and detailed parametrization for the linked region between EG_3 and glutamic group were presented as follows:

(1) **Partial atomic charges**: The RESP (Restrained ElectroStatic Potential) charge fitting method[29] was used to determine the atom charge based on the Hartree−Fock/6-31G* basis set. To maintain compatibility with the CHARMM force field, the aliphatic and aromatic hydrogen charges were constrained to be +0.09 e and +0.15 e, respectively.[27]

(2) **Bond, angle, and dihedral angle**: The MP2/6-31G* basis set was used to calculate the equilibrium values and force constants for all bonds and angles at the linked region. The potential energy surfaces (PES) of the dihedrals were obtained from 360 deg rotational scans. The molecular geometry was fully relaxed at each 10 degrees dihedral angle increment, keeping the selected dihedral angle fixed. The convergence value was set as 0.5 kcal/mol. The obtained parameters were submitted to a PES analysis via the NAMD Energy plug-in of VMD software, which was repeated to acquire the final optimized parameters until all parameters changed by less than one percent.

The Traditional Molecular Dynamics Simulation. The simulation system for the conjugate LPG_n-IFN is much larger than that of apo-IFN, which severely limits the use of simple simulation methods to approach its thermodynamic equilibrium. In this research, an implicit solvent model[30,31] was employed in the traditional molecular dynamics (MD) simulations, and the thermodynamic equilibrium was verified by the following MD with explicit solvent model.

(1) MD simulation with implicit solvent: The generalized Born implicit solvent (GBIS) methodology[32] was employed to describe the solvent effect. The ion concentration and dielectric constant were set as 0.1 mol/L and 78.5, respectively. The system's temperature was maintained at 300 K using the Langevin method.[33] The vdW/electrostatic cutoff, switch, and pairlist were set to 1.2, 1.0 and 1.45 nm, respectively. The simulations were performed on the GBIS system using nonbonded (vdW/electrostatic) cutoff distance of 1.2 nm. A smoothing function was applied to nonbonded forces with a switching cutoff distance of 1.0 nm, and a pair list distance of 1.45 nm. The time step was set as 1 fs,and the number of time step for producing the required trajectories is 10^9, i.e., 1000 ns.

https://doi.org/10.1021/acs.langmuir.3c00501
Langmuir 2023, 39, 6539−6547

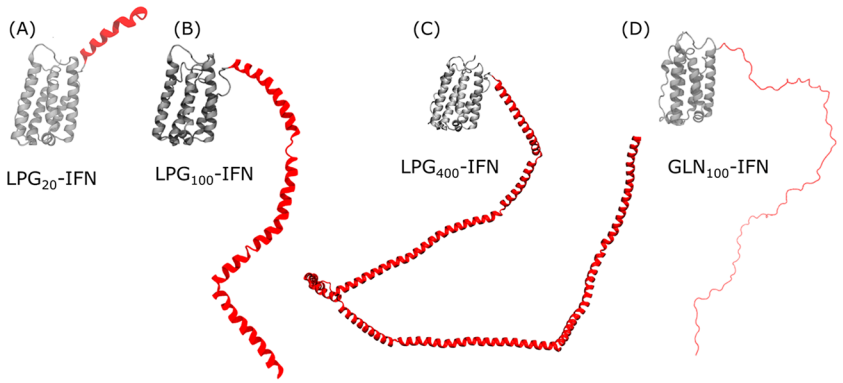

Figure 2. Typical conformations of the interferon conjugates.

(2) MD simulation with explicit solvent: The solvents were explicitly represented by the TIP3P model[34] under periodic boundary conditions (PBC). Na+ and Cl^- were added to make neutralize the system and the salt concentration 0.1 mol/L. The initial atomic coordinates of apo-IFN, LPG_n-IFN, and Glu_{100}-IFN were derived from the last frame of the trajectories simulated with implicit solvent. In an isothermal−isobaric (NPT) ensemble, the system temperature and pressure were maintained at 300 K and 1 bar using the respectively Langevin thermostat and Langevin barostat.[33] The electrostatic interactions were calculated via the Particle mesh Ewald (PME) method.[35] The cutoff of electrostatic and vdW interactions are both 1.2 nm. The simulation box is cubic, and its size is adjusted so that its boundary is more than 1.5 nm away from the protein or conjugates. After energy minimization, 200 ns of traditional MD simulations were performed. The time step was set as 1 fs, and the number of timesteps for producing the required trajectories is 2×10^8. The last 100 ns trajectories were used for data analysis.

The Accelerated Molecular Dynamics Simulation. The energy landscape for macromolecular configuration is so frustrated that the systems are usually trapped in local minimum.[36] The accelerated MD can improve the sampling by adding a bias potential energy to the system without setting the reaction coordinates.[37−39] Four conjugates LPG_n-IFN (n = 20/50/100/200) were further relaxed via accelerated MD simulation. Except for a biased potential energy, other parameters are the same with the traditional MD simulation. The two parameters for accelerated MD in NAMD,[40] V_{dihe} and α_{dihe}, are obtained by the following equations:

$$V_{dihe} = E_{dihe} + (4\ \text{kcal mol}^{-1}\ \text{residue}^{-1} \times N_{frag}) \quad (1)$$

$$\alpha_{dihe} = \frac{1}{5} \times (4\ \text{kcal mol}^{-1}\ \text{residue}^{-1} \times N_{frag}) \quad (2)$$

Here, V_{dihe} and α_{dihe} are given in kcal/mol. α_{dihe} is the actual dihedral torsion potential, and V_{dihe} is the added potential energy. N_{frag} is the total number of fragments of LPG_n-IFN conjugates, where the number of fragments in the EG_3 side chain is the number of repeat units (i.e., 3). E_{dihe} is the average potential energy obtained from the traditional MD simulations with implicit solvent. All the accelerated MD simulations parameters are shown in Table S2 under different systems in the Supporting Information.

Markov State Modeling Analysis. The Markov state modeling (MSM) analysis[41] can identify the critical conformational states and associated transition path between all the sampled conformations.[42] Similar to reaction coordinates in the adaptive sampling process (such as umbrella sampling[43]), the trajectories of accelerated MD simulations were featured from LPG_n-IFN structure features, including center-of-mass distance between polymer chains with IFN, and angles/dihedrals on the backbone of LPG_n-IFN conjugates. The molecular LPG_n-IFN coordinates characterizing each frame of the MD trajectory are transformed into an intuitive basis such as the protein's dihedral angles or contact distance pairs.

We extract two independent components using time-lagged independent component analysis (TICA)[44] using a lag time of 10 ns based on the convergence of time scales. The microstates were grouped further into 5 Macro States using perron-cluster cluster analysis (PCCA) and validated using the Chapman−Kolmogorov criterion.[45] One thousand bootstrapping cycles are used to calculate the statistical errors in thermodynamic and kinetic parameters. Error bars are computed based on a moving block procedure for bootstrapping. The trajectories analysis modules used MDAnalysis[46] and MDTraj.[47] All MSM analysis was performed using PyEMMA.[48]

Molecular Docking and Binding Affinity Analysis. To determine the influence of polyglutamate derivatives on the biological activity of IFN, molecular docking and binding affinity analysis were carried out. First, the best binding sites for apo-IFN and LPG_{20}-IFN were identified via molecular docking with the assistance of HADDOCK (ver. 2.4).[49] The scoring function of HADDOCK is composed of the weighted sum of characteristics, including electrostatic energy, dissolving energy, distance constraint energy, binding energy, VDW energy, and buried surface area. The binding targets are IFN receptors (IFNAR1 and IFNAR2) and human anti-interferon monoclonal antibody Sifalimumab (ABS). The IFN receptors and ABS protein were, respectively, derived from the IFNAR structure (PDB ID: 3SE3) and a crystal structure with 3.00 Å resolution (PDB ID: 4YPG), which has been experimentally demonstrated to bind IFN-α2A effectively.[50,51]

Second, the complex structures with the highest score of HADDOCK were extracted and then thermodynamically relaxed via traditional MD simulations with implicit solvent. The produced trajectories were then used for binding energy analysis via the Molecular mechanics Poisson−Boltzmann surface area (MM/PBSA) method.[52] Details for determining the binding energy via MM/PBSA can be found in our previous papers.[22,53] In brief, the CaFE plugin of VMD[54] was utilized to calculate the binding energy of the receptors (IFNAR1/2) and ligands (LPG_{20}-IFN and apo-IFN) in the gas phase. The APBS module[55] was used to solve the Poisson−Boltzmann equation to determine the solvation polar free energy. The solvent accessible surface area (SASA) was measured to get an estimate of the solvation free energy of the nonpolar part moiety. Finally, the binding free energy was averaged out based on all the conformations. Unless the allosteric process was involved in binding protein to protein, the conformational change of ligand and receptor both before and after binding was relatively minor. Thus, the entropy was disregarded because of the large computational requirement, which was a common strategy for binding energy analysis.[22,53]

Synthesis and Characterization of Free L-P(EG_3Glu)$_n$. Free L-P(EG_3Glu)$_n$ was synthesized by NCA ring-opening polymerization. Taking LPG_{20} as an example, EG_3GluNCA (64 mg, 0.2 mmol, 20 equiv) was dissolved in anhydrous DMF (1.0 mL), mixed with hexamethyldisilazane (HMDS, 1.6 mg, 0.01 mmol, 1.0 equiv) and stirred at room temperature in a glovebox for 12 h. Then the reaction was poured into ethyl ether (50 mL) to obtain a white precipitate.

https://doi.org/10.1021/acs.langmuir.3c00501
Langmuir 2023, 39, 6539−6547

The precipitate was collected by centrifugation, redissolved in water, and freeze-dried to obtain a white colloidal solid, for which the degree of polymerization was characterized by GPC and ^{1}H NMR. LPG_{72} was synthesized by a similar method.

LPG_{20} and LPG_{72} were accurately weighed and dissolved in water to 0.223 and 0.181 mg/mL, respectively. Then the solution was left standing at 4 °C for 12 h to fully dissolve, and the circular dichroism spectrum was characterized. The helicity was calculated using molar ellipticity ($[\theta]$) at 222 nm: helicty % = $(-[\theta] + 3000)/39000 \times 100\%$. Circular dichroism spectroscopy was analyzed on a J-810 CD spectrometer (JASCO, Japan). The light path length of the quartz cell used was 1.0 mm. More details of synthesis and characterization can be found in our previous publication.[15]

RESULTS AND DISCUSSION

Typical Conformations of the Conjugates LPG_n-IFN. Typical conformations of interferon conjugates are presented in Figure 2. Taking LPG_{400}-IFN as an example, the initial structure of LPG_{400} is a long α-helix (Figures S1 and S2 in the Supporting Information). After a thermodynamic relaxation in simulation with implicit solvent, the helical chain of LPG_{400} is broken into multiple short helical segments, and the end-to-end distance of the LPG_{400} chain decreases from the initial 61.5 to 33.4 nm. However, the helical ratio of LPG_{400} is still maintained at a high value (70.1%). To confirm this, the LPG_{400} chain was further relaxed with explicit solvent, and its typical conformation is presented in Figure 2C. The associated end-to-end distance and helical ratio remained at 35.1 nm and 72.3%, respectively. A series of polyglutamic derivatives LPG_n in the conjugate form have been explored, all of which exhibit helical conformations. In contrast, the helical poly(glutamic acid) for the conjugate Glu_{100}-IFN cannot be maintained, and finally it turned out to be an unstructured coil. Because of its hydrophilic side chain, the attached poly(glutamic acid) prefers to be dispersed in aqueous solution rather than on the protein surface.

Will IFN retain its native conformation when being conjugated with the helical LPG_n chain? The deviation of IFN from its native structure is characterized by the parameter "root mean square deviation" (RMSD), which is only 0.18 nm for the simulated apo-IFN (Table S3). After conjugation with Glu_{100}, the RMSD of INF is increased to the maximum 0.49 nm while its helicity is decreased to the minimal 46%, indicating that the hydrophilic coiled chain may not be a good choice for protecting IFN. This is consistent with our previous simulation work:[22] negatively charged Glu tends to interact with water molecules, while positively charged Lys and Arg tend to form contacts with these residues on protein surface.

Notably, the formation of helical structure from coil conformation via atomic MD simulation is extremely CPU-intensive. As an alternate, this work initially constructed the helix structure for all polypeptides, and then performed thermodynamic relaxation to validate the stability of helical structure, which is a commonly used strategy in simulation. Among the simulated conjugates, the helicity of L-P$(EG_3Glu)_n$ should be higher for larger n if the thermodynamic relaxation is insufficient, which is lower in this work (Table S1), reflecting an inherent helical tendency of polyglutamate derivatives.

Driving Forces for the LPG_n Helix. The driving forces for helical structure formation were thoroughly explored. In the case of free LPG_n, their helicities increase continuously with increased chain length (Figure 3A). Further validation is provided from experiments. The secondary structures of the synthesized free LPG_n were detected by circular dichroism

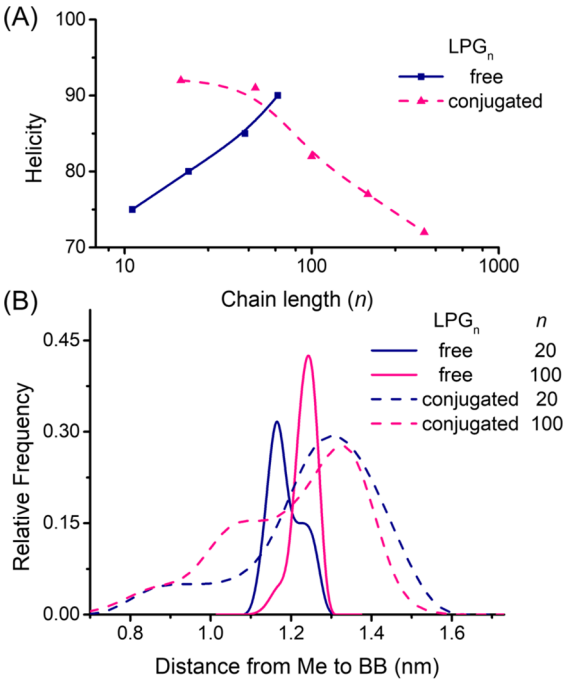

Figure 3. Characterization of the helical LPG_n: (A) Helicity of LPG_n as functions of chain length (n); (B) distance distribution from methyl group (Me) in the EG_3 side chain to its backbone (BB) of LPG_n.

(CD) spectra (Figure S3). The helicity is increased from ~71% to ~105% for the synthesized LPG_{20} and LPG_{72}. This tendency qualitatively verifies the relationship between helicity and chain length found in simulations.

The distances from the methyl group (Me) in the EG_3 side chain to the backbone (BB) of LPG_n are selected as parameters. As shown in Figures 3B and S4, the average distance from Me to BB is higher for longer chain, such as n = 50/100. In our opinion, the two termini of LPG_n provide a lot of free volume for molecular Brownian motion, and many of the EG_3 side chain exist in a coiled form, which is not conducive to dense packing. For longer LPG_n, the proportion of free volume is lower, and the EG_3 side chain can only be arranged in parallel to form a dense packing, thus greatly enhancing the helicity of LPG_n. After conjugated with IFN, LPG_n contains only one terminus, the lower free volume and subsequent parallel arrangement exhibits a higher distance from Me to BB than that of its free form (see Figure 3B). As evidence, the helicity of the conjugated LPG_{20} is 92%, much higher than that of the free form (78%).

However, this tendency is reversed for conjugated LPG_n, and the longer the chain, the lower the helicity, indicating that the steric hindrance from IFN is not conducive to the higher helicity of conjugated LPG_n. As shown in Figure 4A, more atomic contacts are formed between the longer LPG_n and the region Gln^{90}-Leu^{110} of IFN, leading to a shorter distance from IFN to LPG_n. Forced by these attractive interactions, the peptide segment of LPG_{50} near the conjugating site exhibits a β-turn structure (Figure 4B), rather than a straight helical structure.

Periodicity of the helical LPG_n was also investigated, and it was found that LPG_{50} exhibits a periodic variation with respect to the number of atomic contacts between IFN and each EG_3 side chain (see Figure S5A). The sequence number

https://doi.org/10.1021/acs.langmuir.3c00501
Langmuir 2023, 39, 6539−6547

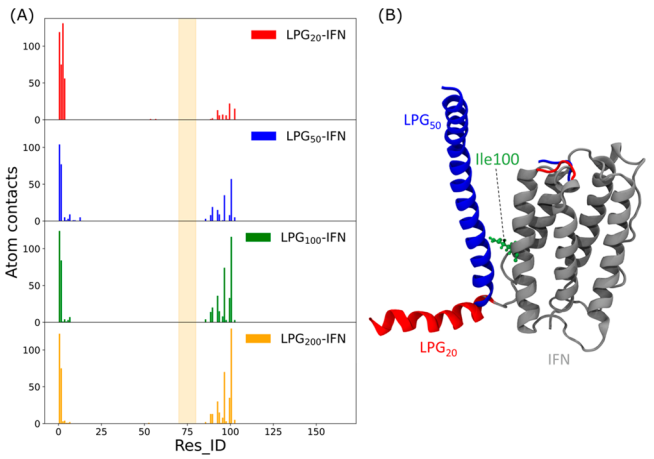

Figure 4. Illustration of the interaction between IFN and LPGn: (A) number of atomic contacts between LPG_n and each residue (Res_ID) of IFN; (B) typical snapshots of LPGn-IFN. In (A), the light-yellow transparent area indicates the region for Loop BC of IFN. In (B), Ile100 of IFN is rendered by the lime CPK representation, loop BC (from Asp71 to Leu80) of IFN and LPGn is , respectively, colored by red and blue for n = 20/50.

corresponding to the curve peak is 4/7/11/14, which indicates that the period (3.5) of LPG_{50} is very close to that of the α-helix (3.6). Thus, the LPG_n helicity is positively influenced by the conjugating site but negatively affected by the steric hindrance caused by IFN, while its periodicity remains unaffected.

In addition, the bending angle and helical probability of each residue in the LPG_n structure were examined using the Bendix module of VMD software[57] (see Figure S6). The results showed that all the bending angles for the shortest LPG_{20} were less than 10 degrees, indicating a straight helical structure. However, the helical structures formed by LPG_{50} and LPG_{100} displayed a curved shape, with the latter even breaking into three segments. Notably, a clear peak in bending angle was observed at position 7 for all simulated LPG_n structures, accompanied by reduced helical probabilities. These observations further highlight the negative impact of steric hindrance on the formation of helical LPG_n structures.

Kataoka and colleagues[58] revealed a coil−helix transition for PEG-*block*-poly(glutamate) copolymer after conjugating it with cisplatin, a hydrophobic drug. Previous research[56] suggested that reducing solvent accessible surface area (SASA) could stabilize the helical structure of polypeptide derivatives. In our opinion, the forces for helix formation should be internally consistent, i.e., local crowding and volume exclusion caused by the aggregation of long side chains, which could also promote protein folding in intracellular solution.[59]

Conformation Variation of IFN after Conjugation. Protein structure is typically more stable when conjugated with a coiled polymer chain, such as PEG. However, it is unclear whether IFN will maintain its native conformation when conjugated with a helical LPG_n chain. To investigate this, we used the parameter RMSD to describe the deviation of IFN from its initial structure (see Table S3). After thermodynamic relaxation, apo-IFN showed minimal deviation with an RMSD of 0.18 nm, falling within the normal range of protein motion. However, as chain length increased, the deviation from the initial structure also increased for LPGn-IFN. The helical LPGn chain appeared ineffective in improving IFN's thermal stability, as conjugation caused a decrease in its helicity from 66% to 53%.

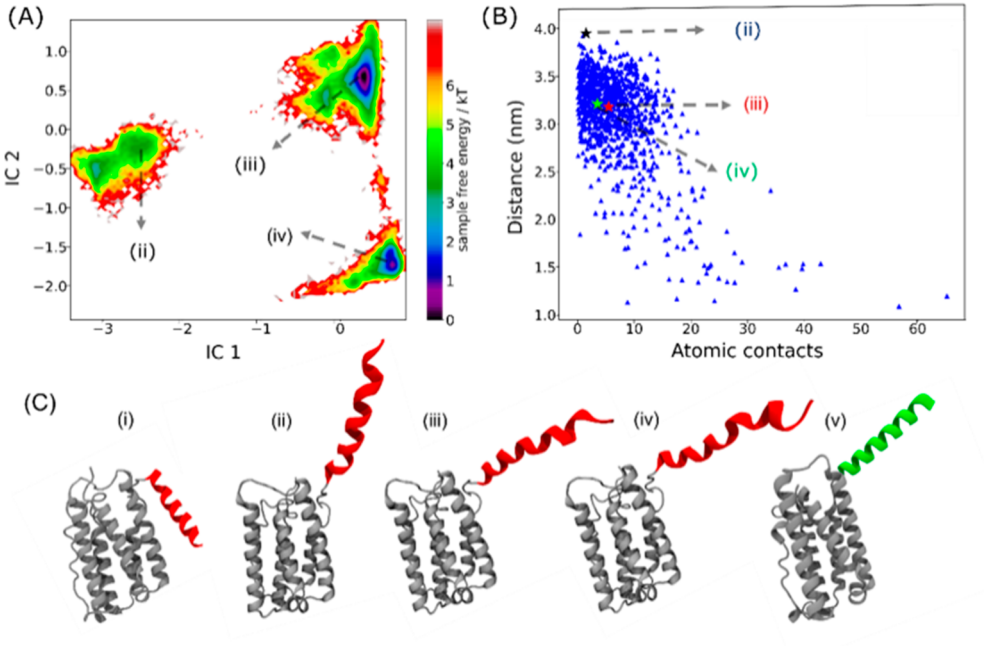

Figure 5. (A) Free energy landscape of LPG_{20}-IFN determined by MSM analysis. (B) Distance from the center-of-mass of IFN to the 20th residue of LPG_{20} as a function of atomic contacts between the region Gln90-Leu110 of IFN and side chain EG_3 of LPG_{20}. (C) Typical snapshots of LPG_{20}-IFN with various orientation: (i) Initial conformation; (ii/iii/iv) conformations corresponding to the local/global minima in (A); (v) conformation of murine interferon predicted by AlphaFold2 (ID: A0A0G2K3I2 in AlphaFold DataBank), and the extra helical segment is colored in green. In (A), the IC1 and IC2 denote the first two time-lagged independent components featured by the center-of-mass distance between LPG_{20} with IFN, and the angles/dihedrals of the backbone of LPG_{20}-IFN conjugates.

https://doi.org/10.1021/acs.langmuir.3c00501
Langmuir 2023, 39, 6539−6547

Despite this, short LPG_n chains (n = 20/50) had a minor influence on IFN's helicity and RMSD, with the IFN structure being very close to its native configuration. The Glu_{100}-IFN system showed lower helicity than apo-IFN and a larger RMSD, implying that the hydrophilic and unstructured Glu_{100} chain had little impact on IFN's thermal stability. Even in the largest LPG_{200}-IFN, the RMSD was only 0.49 nm. Short chains effectively maintained the IFN configuration, while conjugated long chains had a greater effect (see Table S3), disrupting the hydrogen bond network of IFN and leading to a downward trend in its helicity.

Interestingly, an allosteric effect was observed in the Loop BC of IFN, with the distance to the center-of-mass of IFN reduced in the conjugate compared to apo-IFN (see Table S3). The Loop BC region did not contact LPG_n, but the associated interactions caused deformation or displacement of the helix from Asp^{71} to Leu^{80} (see Figure 4). This structural change provided an opportunity for Loop BC to approach the core of IFN, but it might also be a possible reason for the decreased helicity of IFN. In contrast, the Glu_{100}-IFN system exerted little influence on the structure of IFN due to the region's distance from the conjugating site. Dependence on the length of the LPG_n chain was observed, with short LPG_n helical chains showing better stability when conjugated with IFN.

Preferred Direction of the LPG_{20} Helix Relative to IFN. A preferred direction of the LPG_{20} helix relative to IFN was found. For unstructured polymers such as PEG or poly(Glu), there is no fixed orientation relative to the target protein, which may be different for the helical LPG_n. Further exploration through accelerated MD simulation was carried out to achieve a thorough ergodic in the conformation space. Markov state modeling (MSM) analysis (see Figure S7) was used to obtain the free energy landscape. Three popular regions were revealed in the conformation space of LPG_{20}-IFN (Figure 5), and the corresponding conformations are presented as (ii), (iii) and (iv), which also clearly deviates from the initial orientation (see (i) in Figure 5C). Such conformation popularity was also verified by the distance distribution from IFN to the free terminus of LPG_{20} (Figure 5B), which is concentrated in the range [2.8, 3.7 nm] and is about 3.18 nm for conformations (iii) and (iv). On the other hand, their atomic contacts between LPG_{20} and the region Gln^{90}-Leu^{110} of IFN are also in the densest area of contact distribution. In short, such interactions are helpful for reducing system energy, but not for system entropy or the rotation of LPG_{20}. Anyway, the free energy difference between the sampled conformations is very small, allowing orientation adjustment in response to external stimuli, such as receptor recognition.

Notably, the popular conformation of LPG_{20}-IFN is very close to that of murine interferon predicted by the AlphaFold database[60,61] (see (v) in Figure 5C). The sequence and structure of murine interferon are similar to those of IFNα-2A except for its N-terminal region. Compared to IFNα-2A, the N-terminal region of murine Interferon has an extra helical segment with the sequence "MARLCAFLMSLVVMSYW-SACCLG". Interestingly, the residue of murine interferon corresponding to the 20th residue of LPG_{20} is 3.21 nm away from its center of mass, again demonstrating the similarity between these two structures. Such predicted conformation has been further simulated using molecular simulation with explicit solvent, and it demonstrates that the protein's RMSD was maintained at 0.24 nm. The direction of the N-terminal helical segment (Met^1-Gly^{23}) remained consistent and its helicity maintains at 85.7% during the simulation. Overall, murine Interferon demonstrated similar dynamic behavior to the conjugate LPG_{20}-IFN (Figure S8).

Bioactivity of the LPG_{20}-IFN Conjugate. Molecular docking for the popular conformation of LPG_{20}-IFN (i.e., (iii) in Figure 5C) was performed via the HADDOCK 2.4 software.[62] Unexpectedly, the corresponding binding sites between LPG_{20}-IFN and ABS (see Figure S9) are different from those when apo-IFN was docked with ABS (see Figure 6A), and the binding affinity as reflected by the HADDOCK score is changed from −57.1 ± 3.7 kcal/mol to 152.4 ± 17.1 kcal/mol. Such a positive value indicates that the most probable complex may not be stable. While the binding sites of the second probable complex are similar to the apo-IFN/ABS complex (see Figure 6A), the higher HADDOCK score (231.3 ± 15.6 kcal/mol) indicates that the steric repulsion prevents LPG_{20}-IFN from being recognized by ABS.

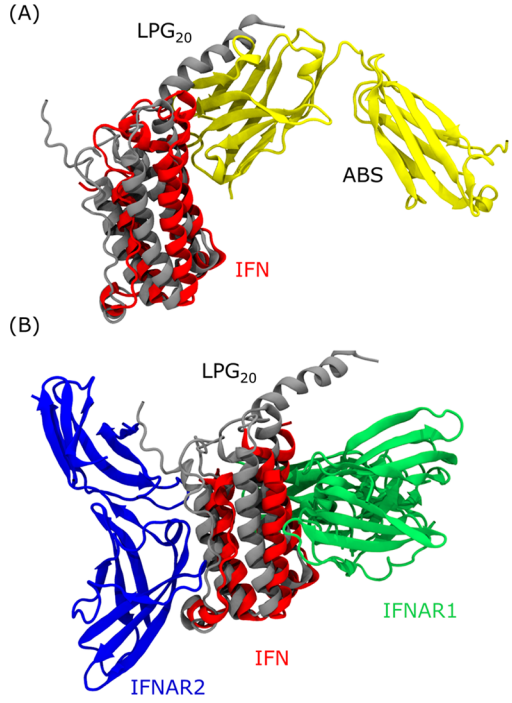

Figure 6. Predicted structure of apo-IFN/LPG_{20}-IFN in complex with (A) antibody sifalimumab (ABS) and (B) its two receptors. Here, apo-IFN and LPG_{20}-IFN are colored in red and gray, respectively; the receptors (IFNAR1 and IFNAR2) are colored in green and blue, respectively; ABS is colored in yellow.

The most probable structures of LPG_{20}-IFN in a complex with its receptors (IFNAR1 and IFNAR2) are presented in Figure 6B, which are similar to these apo-IFN/receptors complexes. These predicted complexes were further relaxed via MD simulation, and the associated binding energies were determined based on MM/PBSA protocol. As shown in Table S4, the binding affinity of apo-IFN to IFNAR1 (−289.5 kJ/mol) is weaker than that to IFNAR2 (−348.3 kJ/mol). After conjugated with the helical LPG_{20}, the binding affinities of IFN to its receptors (IFNAR1 and IFNAR2) respectively decreased to 45% and 67% of the apo-IFN system, but the complex is still stable. Related crystallographic studies[51] reveal that IFNα-2A first binds IFNAR2 and then recruits IFNAR1, while ABS precludes the IFNα-2A/IFNAR1 complex via direct steric

https://doi.org/10.1021/acs.langmuir.3c00501
Langmuir 2023, 39, 6539−6547

hindrance. The atomic contacts between each residue of IFN and its receptor were counted, and Figure S10 reveals that apo-IFN forms more contacts with IFNAR1 than with IFNAR2. In contrast, LPG_{20}-IFN make more atomic contacts with IFNAR2, while the helical LPG_{20} made almost no contact with the IFN receptor.

As we all know, flexible PEG or L-Poly(Glu) can resist adsorption and further recognition of all proteins through chain wobbling. The case is different for helical L-$P(EG_3Glu)_n$. The preferred orientation of L-$P(EG_3Glu)_{20}$ relative to IFN could effectively prevent the binding of ABS to IFN, while not significantly blocking the binding of IFN to its receptor. These insights can also be verified by the experimental results of Hou et al.[15] After conjugated with the helical L-$P(EG_3Glu)_{73}$ and the coiled D,L-$P(EG_3Glu)_{73}$, the circulation half-life of IFN is increased by a factor of 19.2 and 15.6, respectively; while the binding affinity (i.e., IC_{50}) decreased by a factor of 4.2 and 18.8, respectively.[15]

CONCLUSIONS

In summary, the secondary structures of polyglutamate derivatives and their biological activity after conjugation to the target protein (interferon) were investigated by molecular simulation. We found that the local crowding effect induced by the grafted oligoethylene glycols (i.e., EG_3) is the main driving forces for forming the helical structure of L-$P(EG_3Glu)$, and thus the lower proportion of free volume leads to higher helicity. On the other hand, the steric hindrance induced by IFN is not conductive to the helicity of L-$P(EG_3Glu)$ but helpful to its dominant orientation relative to interferon, as revealed by Markov state modeling (MSM) analysis. Subsequent molecular docking and binding energy analysis show that the steric hindrance of attached helical L-$P(EG_3Glu)_{20}$ prevents interferon from being recognized by the neutralizing antibody. In contrast, the complexes between interferon and its receptors remain stable after conjugation with the helical L-$P(EG_3Glu)_{20}$, which is obviously different from the coiled polyglutamate analogues. Collectively, our microscopic exploration rationalizes previous experimental macroscopic phenomena, emphasizing the importance of the helical structure and its relative orientation as control parameters in the updated theoretical framework. The establishment of a new framework requires more simulation and experimental research, and we hope that this work can bring inspiration to the follow-up research.

ASSOCIATED CONTENT

Supporting Information

The Supporting Information is available free of charge at https://pubs.acs.org/doi/10.1021/acs.langmuir.3c00501.

Molecular simulation snapshots, CD data, characterization of the interaction between IFN and the conjugated, MSM analysis of the conformational dynamics, the predicted structure of apo-IFN/LPG_{20}-IFN in complex with ABS and the binding energy for different protein complex (PDF)

AUTHOR INFORMATION

Corresponding Authors

Yantao Chen − *Shenzhen Key Laboratory of Environmental Chemistry and Ecological Remediation, College of Chemistry and Environmental Engineering, Shenzhen University, Shenzhen, Guangdong 518060, China;* orcid.org/0000-0001-8686-1116; Email: ytchen@szu.edu.cn

Hua Lu − *Beijing National Laboratory for Molecular Sciences, Center for Soft Matter Science and Engineering, Key Laboratory of Polymer Chemistry and Physics of Ministry of Education, College of Chemistry and Molecular Engineering, Peking University, Beijing 100871, China;* orcid.org/0000-0003-2180-3091; Email: chemhualu@pku.edu.cn

Authors

Zhuanglin Shen − *Shenzhen Key Laboratory of Environmental Chemistry and Ecological Remediation, College of Chemistry and Environmental Engineering, Shenzhen University, Shenzhen, Guangdong 518060, China; Guangdong Key Laboratory for Biomedical Measurements and Ultrasound Imaging, School of Biomedical Engineering, Shenzhen University Health Science Center, Shenzhen, Guangdong 518060, China*

Yiming Sun − *Beijing National Laboratory for Molecular Sciences, Center for Soft Matter Science and Engineering, Key Laboratory of Polymer Chemistry and Physics of Ministry of Education, College of Chemistry and Molecular Engineering, Peking University, Beijing 100871, China*

Guoliang Zhu − *Shenzhen Key Laboratory of Environmental Chemistry and Ecological Remediation, College of Chemistry and Environmental Engineering, Shenzhen University, Shenzhen, Guangdong 518060, China*

Gaixia Xu − *Guangdong Key Laboratory for Biomedical Measurements and Ultrasound Imaging, School of Biomedical Engineering, Shenzhen University Health Science Center, Shenzhen, Guangdong 518060, China;* orcid.org/0000-0001-9311-0978

Zhenqiang Yu − *Shenzhen Key Laboratory of Environmental Chemistry and Ecological Remediation, College of Chemistry and Environmental Engineering, Shenzhen University, Shenzhen, Guangdong 518060, China;* orcid.org/0000-0002-0862-9415

Complete contact information is available at: https://pubs.acs.org/10.1021/acs.langmuir.3c00501

Author Contributions

The manuscript was written through contributions of all authors. All authors have given approval to the final version of the manuscript.

Notes

The authors declare no competing financial interest.

ACKNOWLEDGMENTS

This study was financially supported by the National Natural Science Foundation of China (Grant No. 22173061 and 22125101).

REFERENCES

(1) Strohl, W. R. Fusion Proteins for Half-Life Extension of Biologics as a Strategy to Make Biobetters. *BioDrugs* **2015**, *29* (4), 215−239.

(2) Ekladious, I.; Colson, Y. L.; Grinstaff, M. W. Polymer−Drug Conjugate Therapeutics: Advances, Insights and Prospects. *Nat. Rev. Drug Discovery* **2019**, *18* (4), 273−294.

(3) Abuchowski, A.; van Es, T.; Palczuk, N. C.; Davis, F. F. Alteration of Immunological Properties of Bovine Serum Albumin by Covalent Attachment of Polyethylene Glycol. *J. Biol. Chem.* **1977**, *252* (11), 3578−3581.

(4) Park, H.; Otte, A.; Park, K. Evolution of Drug Delivery Systems: From 1950 to 2020 and Beyond. *J. Controlled Release* **2022**, *342*, 53−65.
(5) Shi, D.; Beasock, D.; Fessler, A.; Szebeni, J.; Ljubimova, J. Y.; Afonin, K. A.; Dobrovolskaia, M. A. To PEGylate or Not to PEGylate: Immunological Properties of Nanomedicine's Most Popular Component, Polyethylene Glycol and Its Alternatives. *Adv. Drug Delivery Rev.* **2022**, *180*, 114079.
(6) Munasinghe, A.; Mathavan, A.; Mathavan, A.; Lin, P.; Colina, C. M. Molecular Insight into the Protein−Polymer Interactions in N-Terminal PEGylated Bovine Serum Albumin. *J. Phys. Chem. B* **2019**, *123* (25), 5196−5205.
(7) Keefe, A. J.; Jiang, S. Poly(Zwitterionic)Protein Conjugates Offer Increased Stability without Sacrificing Binding Affinity or Bioactivity. *Nat. Chem.* **2012**, *4* (1), 59−63.
(8) Zhang, P.; Liu, E. J.; Tsao, C.; Kasten, S. A.; Boeri, M. V.; Dao, T. L.; DeBus, S. J.; Cadieux, C. L.; Baker, C. A.; Otto, T. C.; Cerasoli, D. M.; Chen, Y.; Jain, P.; Sun, F.; Li, W.; Hung, H.-C.; Yuan, Z.; Ma, J.; Bigley, A. N.; Raushel, F. M.; Jiang, S. Nanoscavenger Provides Long-Term Prophylactic Protection against Nerve Agents in Rodents. *Sci. Transl. Med.* **2019**, *11* (473), eaau7091.
(9) Liu, Y.; Lee, J.; Mansfield, K. M.; Ko, J. H.; Sallam, S.; Wesdemiotis, C.; Maynard, H. D. Trehalose Glycopolymer Enhances Both Solution Stability and Pharmacokinetics of a Therapeutic Protein. *Bioconjugate Chem.* **2017**, *28* (3), 836−845.
(10) Gao, W.; Liu, W.; Mackay, J. A.; Zalutsky, M. R.; Toone, E. J.; Chilkoti, A. In Situ Growth of a Stoichiometric PEG-like Conjugate at a Protein's N-Terminus with Significantly Improved Pharmacokinetics. *Proc. Natl. Acad. Sci. U. S. A.* **2009**, *106* (36), 15231−15236.
(11) Hu, J.; Zhao, W.; Gao, Y.; Sun, M.; Wei, Y.; Deng, H.; Gao, W. Site-Specific in Situ Growth of a Cyclized Protein-Polymer Conjugate with Improved Stability and Tumor Retention. *Biomaterials* **2015**, *47*, 13−19.
(12) Banskota, S.; Yousefpour, P.; Kirmani, N.; Li, X.; Chilkoti, A. Long Circulating Genetically Encoded Intrinsically Disordered Zwitterionic Polypeptides for Drug Delivery. *Biomaterials* **2019**, *192*, 475−485.
(13) Liu, Y.; Yu, P.; Peng, X.; Huang, Q.; Ding, M.; Chen, Y.; Jin, R.; Xie, J.; Zhao, C.; Li, J. Hexapeptide-Conjugated Calcitonin for Targeted Therapy of Osteoporosis. *J. Controlled Release* **2019**, *304*, 39−50.
(14) Zhang, C.; Lu, H. Helical Nonfouling Polypeptides for Biomedical Applications. *Chin. J. Polym. Sci.* **2022**, *40* (5), 433−446.
(15) Hou, Y.; Zhou, Y.; Wang, H.; Sun, J.; Wang, R.; Sheng, K.; Yuan, J.; Hu, Y.; Chao, Y.; Liu, Z.; Lu, H. Therapeutic Protein PEPylation: The Helix of Nonfouling Synthetic Polypeptides Minimizes Antidrug Antibody Generation. *ACS Cent. Sci.* **2019**, *5* (2), 229−236.
(16) Taylor, P. A.; Jayaraman, A. Molecular Modeling and Simulations of Peptide−Polymer Conjugates. *Annu. Rev. Chem. Biomol. Eng.* **2020**, *11* (1), 257−276.
(17) Yang, C.; Lu, D.; Liu, Z. How PEGylation Enhances the Stability and Potency of Insulin: A Molecular Dynamics Simulation. *Biochemistry* **2011**, *50* (13), 2585−2593.
(18) Munasinghe, A.; Mathavan, A.; Mathavan, A.; Lin, P.; Colina, C. M. Atomistic Insight towards the Impact of Polymer Architecture and Grafting Density on Structure-Dynamics of PEGylated Bovine Serum Albumin and Their Applications. *J. Chem. Phys.* **2021**, *154* (7), 075101.
(19) Baker, S. L.; Munasinghe, A.; Murata, H.; Lin, P.; Matyjaszewski, K.; Colina, C. M.; Russell, A. J. Intramolecular Interactions of Conjugated Polymers Mimic Molecular Chaperones to Stabilize Protein−Polymer Conjugates. *Biomacromolecules* **2018**, *19* (9), 3798−3813.
(20) Munasinghe, A.; Baker, S. L.; Lin, P.; Russell, A. J.; Colina, C. M. Structure−Function−Dynamics of α-Chymotrypsin Based Conjugates as a Function of Polymer Charge. *Soft Matter* **2020**, *16* (2), 456−465.
(21) Qiao, Q.; Cai, L.; Shao, Q. Molecular Simulations of Zwitterlation-Induced Conformation and Dynamics Variation of Glucagon-like Peptide-1 and Insulin. *J. Mater. Chem. B* **2022**, *10* (14), 2490−2496.
(22) Liu, Y.; Zhu, G.; Shen, Z.; Chen, Y. Sequence Effect of Peptide-Based Materials on Delivering Interferon-α (IFN-α): A Molecular Dynamic Perspective. *Langmuir* **2022**, *38* (2), 680−688.
(23) Teng, J.; Liu, Y.; Shen, Z.; Lv, W.; Chen, Y. Molecular Simulation of Zwitterionic Polypeptides on Protecting Glucagon-like Peptide-1 (GLP-1). *Int. J. Biol. Macromol.* **2021**, *174*, 519−526.
(24) Huang, J.; Rauscher, S.; Nawrocki, G.; Ran, T.; Feig, M.; de Groot, B. L.; Grubmüller, H.; MacKerell, A. D. CHARMM36m: An Improved Force Field for Folded and Intrinsically Disordered Proteins. *Nat. Methods* **2017**, *14* (1), 71−73.
(25) Phillips, J. C.; Braun, R.; Wang, W.; Gumbart, J.; Tajkhorshid, E.; Villa, E.; Chipot, C.; Skeel, R. D.; Kalé, L.; Schulten, K. Scalable Molecular Dynamics with NAMD. *J. Comput. Chem.* **2005**, *26* (16), 1781−1802.
(26) Kıbrıs, E.; Barbak, N. N.; Irmak, N. E. CHARMM Force Field Generation for a Cationic Thiophene Oligomer with FfTK. *J. Mol. Model.* **2021**, *27* (2), 34.
(27) Vanommeslaeghe, K.; Raman, E. P.; MacKerell, A. D. Automation of the CHARMM General Force Field (CGenFF) II: Assignment of Bonded Parameters and Partial Atomic Charges. *J. Chem. Inf. Model.* **2012**, *52* (12), 3155−3168.
(28) Neese, F. Software Update: The ORCA Program System, Version 4.0. *Wiley Interdiscip. Rev. Comput. Mol. Sci.* **2018**, *8* (1), e1327.
(29) Sigfridsson, E.; Ryde, U.; Bush, B. L. Restrained Point-charge Models for Disaccharides. *J. Comput. Chem.* **2002**, *23* (3), 351−364.
(30) Kleinjung, J.; Fraternali, F. Design and Application of Implicit Solvent Models in Biomolecular Simulations. *Curr. Opin. Struct. Biol.* **2014**, *25*, 126−134.
(31) Onufriev, A. V.; Case, D. A. Generalized Born Implicit Solvent Models for Biomolecules. *Annu. Rev. Biophys.* **2019**, *48* (1), 275−296.
(32) Tanner, D. E.; Chan, K.; Phillips, J. C.; Schulten, K. Parallel Generalized Born Implicit Solvent Calculations with NAMD. *J. Chem. Theory Comput.* **2011**, *7* (11), 3635−3642.
(33) Ceriotti, M.; Bussi, G.; Parrinello, M. Langevin Equation with Colored Noise for Constant-Temperature Molecular Dynamics Simulations. *Phys. Rev. Lett.* **2009**, *102* (2), 020601.
(34) Biswal, P.; Rai, N.; Sharma, K. D. Molecular Dynamics Study of TIP3P, SPC/E and TIP4P Water Models at Room Temperature. MSc Thesis, National Institute of Technology, Rourkela, Rourkela, 2013.
(35) Darden, T.; York, D.; Pedersen, L. Particle Mesh Ewald: An N·log(N) Method for Ewald Sums in Large Systems. *J. Chem. Phys.* **1993**, *98* (12), 10089−10092.
(36) Chen, J.; Wang, W.; Pang, L.; Zhu, W. Unveiling Conformational Dynamics Changes of H-Ras Induced by Mutations Based on Accelerated Molecular Dynamics. *Phys. Chem. Chem. Phys.* **2020**, *22* (37), 21238−21250.
(37) Duan, L.; Guo, X.; Cong, Y.; Feng, G.; Li, Y.; Zhang, J. Z. H. Accelerated Molecular Dynamics Simulation for Helical Proteins Folding in Explicit Water. *Front. Chem.* **2019**, *7*, 540.
(38) Fan, Z.; Siro, T.; Harju, A. Accelerated Molecular Dynamics Force Evaluation on Graphics Processing Units for Thermal Conductivity Calculations. *Comput. Phys. Commun.* **2013**, *184* (5), 1414−1425.
(39) Wang, J.; Alekseenko, A.; Kozakov, D.; Miao, Y. Improved Modeling of Peptide-Protein Bi Through Global Docking and Accelerated Molecular Dynamics Simulations. *Front. Mol. Biosci.* **2019**, *6*, 112.
(40) Wang, Y.; Harrison, C. B.; Schulten, K.; McCammon, J. A. Implementation of Accelerated Molecular Dynamics in NAMD. *Comput. Sci. Discovery* **2011**, *4* (1), 015002.
(41) Konovalov, K. A.; Unarta, I. C.; Cao, S.; Goonetilleke, E. C.; Huang, X. Markov State Models to Study the Functional Dynamics of Proteins in the Wake of Machine Learning. *JACS Au* **2021**, *1* (9), 1330−1341.

https://doi.org/10.1021/acs.langmuir.3c00501
Langmuir 2023, 39, 6539−6547

(42) Pande, V. S.; Beauchamp, K.; Bowman, G. R. Everything You Wanted to Know about Markov State Models but Were Afraid to Ask. *Methods San Diego Calif* **2010**, *52* (1), 99−105.
(43) Kästner, J. Umbrella Sampling. *WIREs Comput. Mol. Sci.* **2011**, *1* (6), 932−942.
(44) Pérez-Hernández, G.; Paul, F.; Giorgino, T.; De Fabritiis, G.; Noé, F. Identification of Slow Molecular Order Parameters for Markov Model Construction. *J. Chem. Phys.* **2013**, *139* (1), 015102.
(45) Röblitz, S.; Weber, M. Fuzzy Spectral Clustering by PCCA+: Application to Markov State Models and Data Classification. *Adv. Data Anal. Classif.* **2013**, *7* (2), 147−179.
(46) Michaud-Agrawal, N.; Denning, E. J.; Woolf, T. B.; Beckstein, O. MDAnalysis: A Toolkit for the Analysis of Molecular Dynamics Simulations. *J. Comput. Chem.* **2011**, *32* (10), 2319−2327.
(47) McGibbon, R. T.; Beauchamp, K. A.; Harrigan, M. P.; Klein, C.; Swails, J. M.; Hernández, C. X.; Schwantes, C. R.; Wang, L.-P.; Lane, T. J.; Pande, V. S. MDTraj: A Modern Open Library for the Analysis of Molecular Dynamics Trajectories. *Biophys. J.* **2015**, *109* (8), 1528−1532.
(48) Scherer, M. K.; Trendelkamp-Schroer, B.; Paul, F.; Pérez-Hernández, G.; Hoffmann, M.; Plattner, N.; Wehmeyer, C.; Prinz, J.-H.; Noé, F. PyEMMA 2: A Software Package for Estimation, Validation, and Analysis of Markov Models. *J. Chem. Theory Comput.* **2015**, *11* (11), 5525−5542.
(49) van Zundert, G. C. P.; Rodrigues, J. P. G. L. M.; Trellet, M.; Schmitz, C.; Kastritis, P. L.; Karaca, E.; Melquiond, A. S. J.; van Dijk, M.; de Vries, S. J.; Bonvin, A. M. J. J. The HADDOCK2.2 Web Server: User-Friendly Integrative Modeling of Biomolecular Complexes. *J. Mol. Biol.* **2016**, *428* (4), 720−725.
(50) Thomas, C.; Moraga, I.; Levin, D.; Krutzik, P. O.; Podoplelova, Y.; Trejo, A.; Lee, C.; Yarden, G.; Vleck, S. E.; Glenn, J. S.; Nolan, G. P.; Piehler, J.; Schreiber, G.; Garcia, K. C. Structural Linkage between Ligand Discrimination and Receptor Activation by Type I Interferons. *Cell* **2011**, *146* (4), 621−632.
(51) Oganesyan, V.; Peng, L.; Woods, R. M.; Wu, H.; Dall'Acqua, W. F. Structural Insights into the Neutralization Properties of the Fully Human, Anti-Interferon Monoclonal Antibody Sifalimumab. *J. Biol. Chem.* **2015**, *290* (24), 14979−14985.
(52) Miller, B. R.; McGee, T. D.; Swails, J. M.; Homeyer, N.; Gohlke, H.; Roitberg, A. E. MMPBSA.Py: An Efficient Program for End-State Free Energy Calculations. *J. Chem. Theory Comput.* **2012**, *8* (9), 3314−3321.
(53) Chen, Y.; Wang, J.; Zhang, J.; Wang, W. Binding Modes of Bcl-2 Homology 3 (BH3) Peptides with Anti-Apoptotic Protein A1 and Redesign of Peptide Inhibitors: A Computational Study. *J. Biomol. Struct. Dyn.* **2018**, *36* (15), 3967−3977.
(54) Liu, H.; Hou, T. CaFE: A Tool for Binding Affinity Prediction Using End-Point Free Energy Methods. *Bioinformatics* **2016**, *32*, 2216−2218.
(55) Jurrus, E.; Engel, D.; Star, K.; Monson, K.; Brandi, J.; Felberg, L. E.; Brookes, D. H.; Wilson, L.; Chen, J.; Liles, K.; Chun, M.; Li, P.; Gohara, D. W.; Dolinsky, T.; Konecny, R.; Koes, D. R.; Nielsen, J. E.; Head-Gordon, T.; Geng, W.; Krasny, R.; Wei, G.-W.; Holst, M. J.; McCammon, J. A.; Baker, N. A. Improvements to the APBS Biomolecular Solvation Software Suite. *Protein Sci.* **2018**, *27* (1), 112−128.
(56) Hamed, E.; Xu, T.; Keten, S. Poly(Ethylene Glycol) Conjugation Stabilizes the Secondary Structure of α-Helices by Reducing Peptide Solvent Accessible Surface Area. *Biomacromolecules* **2013**, *14* (11), 4053−4060.
(57) Dahl, A. C. E.; Chavent, M.; Sansom, M. S. P. Bendix: Intuitive Helix Geometry Analysis and Abstraction. *Bioinformatics* **2012**, *28* (16), 2193−2194.
(58) Mochida, Y.; Cabral, H.; Miura, Y.; Albertini, F.; Fukushima, S.; Osada, K.; Nishiyama, N.; Kataoka, K. Bundled Assembly of Helical Nanostructures in Polymeric Micelles Loaded with Platinum Drugs Enhancing Therapeutic Efficiency against Pancreatic Tumor. *ACS Nano* **2014**, *8* (7), 6724−6738.
(59) Perry, S. L. Phase Separation: Bridging Polymer Physics and Biology. *Curr. Opin. Colloid Interface Sci.* **2019**, *39*, 86−97.
(60) Jumper, J.; Evans, R.; Pritzel, A.; Green, T.; Figurnov, M.; Ronneberger, O.; Tunyasuvunakool, K.; Bates, R.; Žídek, A.; Potapenko, A.; Bridgland, A.; Meyer, C.; Kohl, S. A. A.; Ballard, A. J.; Cowie, A.; Romera-Paredes, B.; Nikolov, S.; Jain, R.; Adler, J.; Back, T.; Petersen, S.; Reiman, D.; Clancy, E.; Zielinski, M.; Steinegger, M.; Pacholska, M.; Berghammer, T.; Bodenstein, S.; Silver, D.; Vinyals, O.; Senior, A. W.; Kavukcuoglu, K.; Kohli, P.; Hassabis, D. Highly Accurate Protein Structure Prediction with AlphaFold. *Nature* **2021**, *596* (7873), 583−589.
(61) Varadi, M.; Anyango, S.; Deshpande, M.; Nair, S.; Natassia, C.; Yordanova, G.; Yuan, D.; Stroe, O.; Wood, G.; Laydon, A.; Žídek, A.; Green, T.; Tunyasuvunakool, K.; Petersen, S.; Jumper, J.; Clancy, E.; Green, R.; Vora, A.; Lutfi, M.; Figurnov, M.; Cowie, A.; Hobbs, N.; Kohli, P.; Kleywegt, G.; Birney, E.; Hassabis, D.; Velankar, S. AlphaFold Protein Structure Database: Massively Expanding the Structural Coverage of Protein-Sequence Space with High-Accuracy Models. *Nucleic Acids Res.* **2022**, *50* (D1), D439−D444.
(62) de Vries, S. J.; van Dijk, M.; Bonvin, A. M. J. J. The HADDOCK Web Server for Data-Driven Biomolecular Docking. *Nat. Protoc.* **2010**, *5* (5), 883−897.

https://doi.org/10.1021/acs.langmuir.3c00501
Langmuir 2023, 39, 6539−6547